# Curvature effects on valley splitting and degeneracy lifting: Case of Si/Ge rolled-up nanotubes

Giovanni Pizzi,[1,2,*] Michele Virgilio,[2,3] Giuseppe Grosso,[2,3] Suwit Kiravittaya,[4,†] and Oliver G. Schmidt[4]
[1]*Scuola Normale Superiore, Piazza dei Cavalieri 7, I-56126 Pisa, Italy*
[2]*NEST, Istituto Nanoscienze-CNR, Piazza San Silvestro 12, I-56127 Pisa, Italy*
[3]*Dipartimento di Fisica "E. Fermi," Università di Pisa, Largo Pontecorvo 3, I-56127, Pisa, Italy*
[4]*Institute for Integrative Nanosciences, IFW Dresden, Helmholtzstrasse 20, D-01069 Dresden, Germany*
(Received 31 October 2011; published 8 February 2012)

We numerically investigate electronic states, degeneracy lifting, and valley splitting in the conduction band of rolled-up Si/Ge nanotubes. Results are derived from a tight-binding model where the input equilibrium positions of the atoms are obtained by means of continuum elasticity theory. We find three inequivalent $\Delta$ valleys. The lifting of their energy degeneracy and the spatial distribution of the corresponding states are interpreted in terms of nonbiaxial strain and confinement effects. The intervalley interaction in Si/Ge nanotubes is studied as a function of the thickness and curvature of the tube. We demonstrate that the curvature affects the intervalley interaction, in close analogy to what happens with the application of a perpendicular electric field in planar quantum well Si/Ge systems.

DOI: 10.1103/PhysRevB.85.075308 PACS number(s): 73.22.−f, 73.21.−b, 68.65.−k

## I. INTRODUCTION

In the last years, significant research efforts have been oriented toward the exploitation of curvature effects to tailor the mechanical, electronic, transport, and optical properties of different classes of nanostructures, as, for instance, carbon nanotubes,[1,2] nanocorrugated thin films,[3–8] and rolled-up nanotubes.[9–15] In particular, rolled-up nanotubes, originating from the self-scrolling of a differentially stressed film when released from a substrate, have recently proven to be particularly promising for the design of new functional devices.[12,13,16–21] With the aim of engineering the electronic properties of the tubes, a preliminary theoretical study is of the uttermost importance. To the best of our knowledge, only recently a few theoretical studies of the electronic properties of rolled-up tubes have appeared,[7,22–25] but they all use a continuum approach ($k \cdot p$ with effective mass), while a complete atomistic calculation of the electronic band structure over the whole Brillouin Zone (BZ) capturing all the relevant features is still lacking.

In epitaxial systems, the strain field resulting from the scrolling accounts for the most important effects on their electronic properties.[26,27] In particular, in tube systems, the nonbiaxial strain field resulting from the scrolling breaks the equivalency of the two orthogonal lines locally perpendicular to the radial direction, which would be otherwise degenerate in the case of planar geometry (for lattices with tetragonal symmetry). Moreover, for Si material, it is expected that the confinement of carriers perpendicular to the tube radius produces a valley splitting (VS) interaction, where the interface or the confining potential produces a coupling between states which are degenerate in the bulk. This effect has a long-lasting story since the first measurements in Si inversion layers,[28] followed by studies in quantum well and superlattice structures[29–35] and, more recently, in other low-dimensional structures, as for instance quantum dots.[36] It is well known that Si-based systems showing VS effects have been indicated as promising candidates for quantum computation schemes,[37,38] since Si is expected to have longer spin coherence times for conduction electrons than GaAs. For this reason VS has been exploited in conjunction with Zeeman splitting to produce (in suitably designed systems) a nondegenerate ground state, hence removing the main source of decoherence. Moreover, it has been shown that the magnitude of the VS can be tuned by means of an external electric field.[30,31,34]

In this paper, we calculate the electronic structure of Si/Ge rolled-up nanotubes in the whole conduction band, and compare it with the one of corresponding planar slab structures. We discuss how the main features of the lowest conduction bands originate from the bulk band structure in terms of folding, strain, and confinement effects. On this basis, the lifting of the degeneracy of the $\Delta$ valleys along the different directions in $k$ space is explained. We then investigate the intervalley interaction of the lowest conduction states and how the VS is influenced by the tube curvature, showing that the effects of the nonuniform strain due to the curvature are analogous to those caused by a superimposed gate field in an equivalent planar quantum well (QW) structure. Our theoretical description is based on the continuum elasticity theory (CET)[39] for the geometry optimization of the atomic positions in the tube; the electronic properties in the whole BZ are calculated by means of an atomistic $sp^3d^5s^*$ tight-binding (TB) Hamiltonian model, appropriately adapted to describe the discrete cylindrical symmetry.

This paper is organized as follows. We first introduce in Sec. II basic elements for the real- and $k$-space description of the tube. This allows us to interpret the effects due to the nonuniform strain field induced by the curvature on the band structure of the tube. Some technical details on the role of the strain field are examined in the Appendix. In this section we discuss also how the equilibrium position of the atoms are numerically evaluated and introduce the tight-binding (TB) model adopted for the calculation of the electronic states. In Sec. III we present the band structure of a typical tube system, focusing on the main features of the conduction band (CB) and on the intervalley splitting of the states at its bottom. A comparison with similar results obtained in the corresponding planar slab structure are also reported. Finally we discuss the effects of the tube thickness and curvature on the valley

 ©2012 American Physical Society

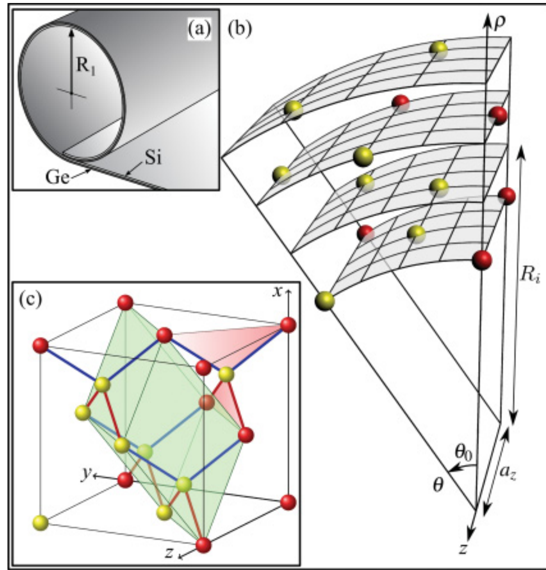


FIG. 1. (Color online) (a) Sketch of a rolled-up Si-Ge tube; $R_1$ is the radius of the first shell of Si atoms. (b) Chosen unit cell for the tube with two atoms on each plane (yellow balls) evidencing the discrete rotational symmetry around the $z$ axis. Each red ball represents an atom that can be reached from the appropriate yellow ball on the same shell by means of discrete translations along (or discrete rotations around) $z$. (c) Conventional unit cell for a bulk diamond lattice (black cube) with eight atoms (yellow balls), from which the curved tube cell (b) originates. The green shaded region represents the primitive cell of the diamond lattice, containing only two atoms. Planes defined by couples of first-neighbor bonds are shaded in pink (see text).

splitting (VS) for the lowest-energy conduction states. Our conclusions are drawn in Sec. IV.

## II. SYSTEM DESCRIPTION AND METHOD

We consider $Si_{N_{Si}}/Ge_{N_{Ge}}$ rolled-up tubes [see sketch in Fig. 1(a)], i.e., tubes composed of $N_{Si}$ monolayers (MLs) of Si and $N_{Ge}$ MLs of Ge, grown along the [001] direction. Inner and outer dangling bonds are passivated with H atoms. Here a ML is defined as a single atomic plane orthogonal to the [001] direction, so that the distance between the MLs in the unstrained bulk crystal is $a_0/4$, where $a_0$ is the unstrained lattice constant of the crystal. By choosing the unit cell of Fig. 1(b), we are assuming perfect periodic conditions not only for translations of integer multiples of $a_z$ along the $z$ axis, but also for rotations of integer multiples of $\theta_0 = 2\pi/N_\theta$ around the $z$ axis ($N_\theta$ gives the number of cells along $\theta$). The above assumption of cylindrical symmetry is a good approximation of the real rolled tube structure for what concerns the study of its electronic properties and in particular of the strain effects on the band structure, since even the smallest tubes considered here have $N_\theta > 550$ and then one expects that the electronic spectrum is not substantially modified by the presence of the overlap rolling region sketched in Fig. 1(a).

In order to calculate the electronic properties of the tube by means of the TB method, we need the atomic positions as input parameters. To this aim, taking the relevant parameters (elastic constants and lattice constants) from Ref. 40, we minimize the total elastic energy of the system exploiting the linear CET for the curved geometry.[41,42] The outcomes of the calculation are the tube radius and the local strain status, defined in cylindrical coordinates by the diagonal components of the strain tensor $\epsilon_{\rho\rho}(\rho)$, $\epsilon_{\theta\theta}(\rho)$, $\epsilon_{zz}(\rho)$, which are functions of the radial coordinate $\rho$ (the off-diagonal components of the strain tensor are zero). We stress that, since the lattice constant $a_{Si}$ of Si is smaller than $a_{Ge}$, and we are neglecting intrinsic surface effects such as reconstructions,[11] we find that the Si region is in the inner side of the rolled-up tube, as shown in Fig. 1(a). The tube radius and the strain tensor determine the atomic positions within the chosen unit cell of the tube [Fig. 1(b)], which can be obtained from the bulk undistorted diamond-lattice cell shown in Fig. 1(c). To exploit the cylindrical symmetry of the tube, it is convenient to choose as a unit cell the conventional cell [black cube of Fig. 1(c)], specified by the fundamental vectors along the [100], [010], [001] directions. The tube cell of Fig. 1(b) can then be obtained associating the $x$ ($y$) direction to the $\rho$ ($\theta$) direction, curving the cell, and then stacking $N_{Si} + N_{Ge}$ atomic shells along $\rho$. Note that the unit cell of Fig. 1(c) contains two atoms (yellow balls) for each plane orthogonal to the growth direction ($x$), and the same holds for the tube cell of Fig. 1(b). All other atoms (red balls in the figures) can be reached by lattice translations or rotations. In the tube unit cell, the radial coordinates of the shells are indicated by $R_i$, $i = 1,2,\ldots,N_{Si} + N_{Ge}$ and are evaluated from the $\epsilon_{\rho\rho}(\rho)$ strain component obtained from the CET calculation. In particular, $R_1$ represents the radial coordinate of the most internal shell of Si atoms. In Ref. 41 it has been shown that to first order in the strain field, it makes no difference for the radius if $a_z$ takes a relaxed value or it is equal to $a_{Si}$. Moreover, we have verified that the structural relaxation of the tube along the $z$ axis does not significantly change the atomic positions, the electronic spectrum, and the values of the valley splitting of the doublet at the bottom of the conduction band. For these reasons, throughout this work we assume $a_z = a_{Si}$.

To interpret the band structure of the tubes, we first describe how the eigenenergies of the electrons in bulk Si fold into the BZ of the tube. The BZ of the (minimal) diamond-lattice primitive cell [green cell in Fig. 1(c)] is the truncated octahedron,[43] represented by black solid lines in Fig. 2(a). On the other hand, if we consider the conventional cell of Fig. 1(c) containing eight atoms, the corresponding BZ results to be the cube shaded in Fig. 2(a) with vertices at the $L$ points. Therefore, to map the bulk band structure obtained in the usual (minimal) representation into the one presently adopted, one has to fold the truncated octahedron into the shaded cubic region of Fig. 2(a). In the case of a planar slab with finite thickness in the $x$ direction (i.e., an "unrolled" tube), $k_x$ is no longer a good quantum number and the corresponding BZ is obtained from the projection of the three-dimensional bulk BZ onto the $yz$ plane, reducing to the two-dimensional dark rectangle of Fig. 2(b). Similar considerations also apply for the tube geometry, and the BZ in the $(k_\theta,k_z)$ space is again the rectangle sketched in Fig. 2(b). Note, however, that in this case the discrete rotational symmetry implies that $k_\theta$ can assume only $N_\theta$ integer values. For the following, it is useful to define three high-symmetry points in the tube BZ: the $\Gamma$ point at the origin, and the $\Theta$ and $Z$ points located at the zone

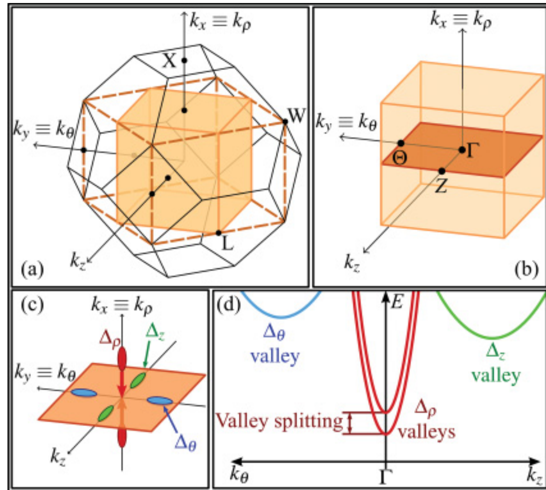


FIG. 2. (Color online) (a) Brillouin zone (black lines) of the bulk diamond primitive cell. The shaded cube with vertices at the $L$ points is the BZ corresponding to the conventional unit cell (see text). The dashed lines are a guide to the eye. (b) Folding of the bulk BZ onto the two-dimensional BZ (dark orange rectangle) for the planar slab, or equivalently for the tube structure. (c) Ellipsoids of constant energy around the six $\Delta$ minima of the bulk Si (or Ge) crystal structure. The two conjugated $\Delta_\rho$ minima (red) fold into the $\Gamma$ point of the 2D BZ of the tube. (d) Schematic of the CB electronic structure of a Si-Ge tube, adopting the same colors of panel (c). The two conjugated $\Delta_\rho$ valleys fold into $\Gamma$ and their degeneracy is resolved due to the VS interaction. The two conjugated $\Delta_\theta$ valleys remain unfolded and do not interact; the same holds for the $\Delta_z$ valleys.

boundaries along the $k_\theta$ and $k_z$ directions, respectively; the band structures reported in the following are plotted along the $\Theta$-$\Gamma$-$Z$ path.

The different valley minima in the conduction band of the tube can be qualitatively interpreted in terms of the bulk electronic structure and its modifications due to band offsets, confinement, folding, and strain effects. In particular, the lowest conduction-band states of the tube originate from the $\Delta$ minima along the six $\Gamma$-$X$ lines of the strained Si and Ge layers [the $X$ point is indicated in Fig. 2(a)]. Indeed, we have verified that for the geometric configurations investigated in this paper, the states of the tube that originate from bulk $L$ and $\Gamma$ minima are much higher in energy (this fact is due both to the band offsets at the Si/Ge interface and to the low $\Gamma$ and $L$ confinement masses). To illustrate the folding of the $\Delta$ states in the case of a finite slab or a tube with periodicity along $y \equiv \theta$ and along $z$ we show in Fig. 2(c) the corresponding ellipsoids of constant energy. It is then apparent that the four $\Delta_\theta$ and $\Delta_z$ minima remain unfolded, while the two conjugated $\Delta_\rho$ valleys fold at $\Gamma$. Moreover, for what concerns the confinement effects, we notice that the six $\Delta$ states have different effective masses along the confinement direction $x \equiv \rho$ [see Fig. 2(c)]. In fact, the confinement mass of the $\Delta_\rho$ states is larger than the mass of $\Delta_\theta$ and $\Delta_z$ states, and then a smaller confinement energy for the (folded) $\Delta_\rho$ electrons is expected.

It is important to include in this picture also strain effects which significantly contribute in determining the relative positions of the different valley minima. In the investigated Si/Ge tubes, the strain component $\epsilon_{zz}$ is constant and negative in the Ge region (compressive strain) whereas it vanishes in the Si layers (since $a_z = a_{\mathrm{Si}}$). On the other hand, the strain field along the $\theta$ and $\rho$ directions is layer dependent. For typical geometries, $\epsilon_{\theta\theta}(\rho)$ [$\epsilon_{\rho\rho}(\rho)$] increases (decreases) almost linearly with $\rho$ except at the interface and has a negative (positive) discontinuity at the Si/Ge interface, as discussed in detail in the Appendix for an exemplificative case. Thus, although $\Delta_z$ and $\Delta_\theta$ electrons have the same confinement mass, we expect that the respective energies differ in the curved geometry, becoming equal only in the limit case $R_1 \to \infty$ (planar slab). For the interpretation of the results discussed in the following it is worthwhile to remind here that a compressive (tensile) component of the strain along the $z$ or $\theta$ directions determines a lowering (rise) in energy of the $\Delta$ states along the same directions. Finally, analogously to what happens in QW systems,[28,29,38,44–46] we expect that the two (folded) $\Delta_\rho$ conjugated valleys in the $\rho$ direction interact through the interface potential. Consequently, due to this intervalley interaction, the degeneracy of the two $\Delta_\rho$ minima is lifted and a doublet of states originates at the $\Gamma$ point, where for the chosen unit cell the bottom of the conduction band is located. From all the previous considerations, we expect for the lowest CB of the tube a structure similar to that schematically shown in Fig. 2(d).

The quantitative evaluation of the tube band structure and of the valley splitting effect was performed by means of a TB model with $sp^3d^5s^*$ orbital basis set and first-neighbors interactions. We chose the curved unit cell discussed above with the appropriate periodic boundary conditions along the $z$ and $\theta$ directions. Since in this work we are concerned with the conduction-band states only, we can safely neglect the spin-orbit interaction. For the hopping and self-energies in Si and Ge we adopted the TB parametrization of Niquet *et al.*,[47] which also provides the interaction parameters for the mixed Si-Ge bonds at the interfaces. Moreover, the parametrization of Ref. 47, unlike most of the works reported in the literature, allows us to take into account strain effects due to generic (i.e., not biaxial) strain fields, as it is the case in the curved geometry studied here. For the dangling bonds at the innermost and outermost layers, which are passivated with hydrogen atoms, we used the TB parameters provided by Zheng *et al.*[48] More technical details of the method will be reported in a forthcoming paper.

## III. CONDUCTION BAND AND VALLEY SPLITTING OF SIGE NANOTUBES

As an exemplificative case, in Fig. 3 we show the conduction-band structure of a tube with $N_{\mathrm{Si}} = 16$ and $N_{\mathrm{Ge}} = 9$, which are realistic values for the growth of rolled-up Si/Ge tubes.[9,10,49] The corresponding equilibrium radius of the inner Si layer is $R_1 = 49.1$ nm. For comparison, in Fig. 3 the band structure of a planar $\mathrm{Si}_{16}/\mathrm{Ge}_9$ slab, obtained in the limit $R_1 \to \infty$, is also shown. In both band structures, near-gap states are related to the three kinds of $\Delta$ valleys as schematized in Fig. 2(d); note the VS doublet due to the $\Delta_\rho$ states folded at the BZ center. At higher energies, the bands become very complicated due to the presence and mixing of states with different symmetries, excited states, etc. Nevertheless, the adoption of a TB Hamiltonian with a rich basis set ensures

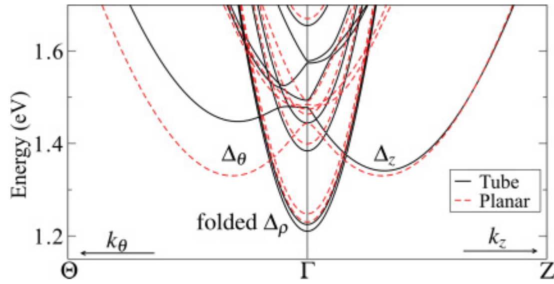


FIG. 3. (Color online) Conduction-band structure of a $Si_{16}/Ge_9$ tube (black solid lines) along the $\Theta$-$\Gamma$-$Z$ path. The internal radius of this tube is $R_1 = 49.1$ nm. The band structure of a $Si_{16}/Ge_9$ planar slab ($R_1 \to \infty$) grown on a Si buffer is also reported with red dashed lines.

that in the whole energy range of Fig. 3 our description of the electronic states remains accurate.

The main difference between the band structures of the planar slab and of the tube shown in Fig. 3 is the shift to higher energy of the $\Delta_\theta$ valley of the tube with respect to the corresponding states in the slab. Indeed, as already mentioned, while in the slab the $\Delta_\theta$ and $\Delta_z$ valleys have the same energy, this degeneracy is lifted in the tube by the different strain field along the $\theta$ and $z$ directions. In fact (see discussion in the Appendix) the band-edge effective potential of the $\Delta_\theta$ electrons, which has a triangular shape in the radial direction, is determined by the strain field and in particular by the $\epsilon_{\theta\theta}(\rho)$ component along $\theta$. This strain potential confines the lowest $\Delta_\theta$ states in the Si region of the tube [see Fig. 5(d)] and a larger confinement energy with respect to the $\Delta_z$ states is obtained.

We now focus on the VS of the lowest doublet at $\Gamma$. The typical features predicted for the intervalley interaction in Si/SiGe QW systems are present also in this context, but peculiar differences related to the curved geometry are predicted. In fact, the curvature determines the strain potential, which in turn influences the VS with effects analogous to the application of a static electric field along the growth direction in planar Si/SiGe QW systems. To clarify this point we report in Figs. 4(a)–4(c) the squared moduli of the wave functions calculated at the $\Gamma$ point, as a function of the radial coordinate, for three tubes with $N_{Si} = 40$ and different curvatures, corresponding to $N_{Ge} = 22$, 85, and 123, respectively. Both the ground and the first excited VS doublets are visible in the panels. Note that in these plots the $\rho$ coordinate extends mainly in the Si region [central white area in Figs. 4(a)–4(c)], where the wave functions are different from zero. In fact, the Ge region (located at the right side of the plots) acts as a barrier since the CB offset at the Si/Ge interface is about 0.7 eV; the layer of H atoms passivating the inner surface is on the left of the Si region. Due to the curvature, in the Si region $\epsilon_{\rho\rho}(\rho)$ decreases with $\rho$. We have numerically verified that the dependence of $\epsilon_{\rho\rho}(\rho)$ on $\rho$ is almost linear. It follows that also the band-edge profile for the $\Delta_\rho$ electrons varies linearly and has the shape of a triangular potential [see Figs. 4(a)–4(c)] just as it happens when a static electric field is applied to a planar QW structure along its growth direction. For fixed $N_{Si}$, the change of $N_{Ge}$ is then a way to tune the curvature and then the gradient of $\epsilon_{\rho\rho}(\rho)$, which controls the band bending or equivalently the effective vertical electric

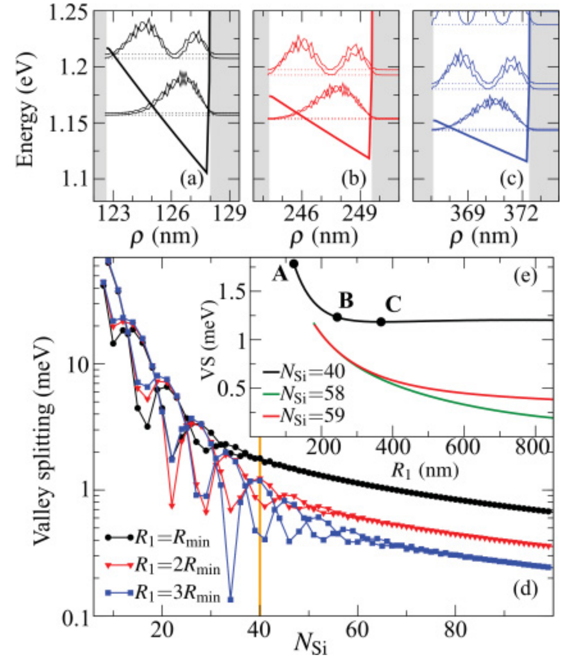


FIG. 4. (Color online) (a)–(c) Squared moduli of the wave functions, calculated at the $\Gamma$ point, for tubes with $N_{Si} = 40$, and internal radius $R_1 = R_{min}$, $R_1 = 2R_{min}$, and $R_1 = 3R_{min}$, respectively. The corresponding values for $N_{Ge}$ are 22, 85, 123. The triangular band profiles for the $\Delta_\rho$ valleys are also shown. The white central area represents the Si region; the left (inner side) is made of the H passivation layer; the Ge region in on the right side. (d) VS of the ground-state doublet at $\Gamma$ as a function of $N_{Si}$. The value of $N_{Ge}$ is chosen in order to obtain the minimum internal radius of the tube $R_1 = R_{min}$ (black dots), $R_1 = 2R_{min}$ (red triangles), or $R_1 = 3R_{min}$ (blue squares); see text. The lines, connecting points with even or odd $N_{Si}$, are only a guide to the eye. The vertical orange line indicates the value of $N_{Si}$ for which panels (a)–(c) are calculated. (e) VS of the ground-state doublet at $\Gamma$ as a function of the tube internal radius $R_1$, for three different values of $N_{Si}$. Each curve starts from the minimum attainable value for $R_1$. The black dots labeled A, B, and C refer to the systems of panels (a), (b), and (c), respectively.

field. Indeed, very large values of $N_{Ge}$ correspond to large values of the tube radius $R_1$ and then to modest strain gradients or equivalently band-edge bendings. On the other hand, when $N_{Ge} \to 0$ we obtain a Si planar slab, i.e., $R_1 \to \infty$. We thus expect that, for each value of $N_{Si}$, there is a unique value of $N_{Ge}$ that minimizes the tube radius: we call this minimum radius $R_1 = R_{min}$, which of course depends only on $N_{Si}$.

Since the wave functions corresponding to the ground-state doublet are confined mainly in the Si region, it is interesting to plot the VS of the ground-state doublet at $\Gamma$ as a function of $N_{Si}$, for the minimum radius $R_1 = R_{min}$ [black squares in Fig. 4(d)]. For comparison in Fig. 4(d) we also show the VS data calculated for two and three times this value (red and blue data points, respectively). Again, the results of Fig. 4 can be interpreted in close analogy to VS data obtained for planar QW systems under different bias (see, for instance, Fig. 1 of Ref. 34). For sufficiently small values of $N_{Si}$ we find the typical oscillations of the VS amplitude as a function of the number of monolayers in the well region. This oscillating behavior and the related period are in agreement with similar results reported

for rectangular Si/SiGe QW systems with sharp interfaces, for which the VS amplitude has been predicted[45] to oscillate as a function of $N_{\mathrm{Si}}$ as $(N_{\mathrm{Si}}+2)^{-3}|\sin[(N_{\mathrm{Si}}+2)\varphi_{\min}]|$, where $\varphi_{\min}$ depends on the position of the valley minimum $k_0$ along the $\Delta$ line of bulk silicon. Note that in Fig. 4(d) the VS oscillations have been emphasized connecting even and odd $N_{\mathrm{Si}}$ data points as a guide to the eye. In fact, the valley splitting depends strongly on the details of the interfaces defining the confinement region. Since bonds connecting first neighbors on adjacent planes are rotated by 90° when moving from one ML to the next one [see pink shaded regions of Fig. 1(c)], the direction of the H-Si bonds at the inner interface of the Si region is parallel (orthogonal) to the direction of the Si-Ge bonds at the outer interface if $N_{\mathrm{Si}}$ is even (odd). This fact introduces a phase shift between the VS oscillations calculated for even and odd $N_{\mathrm{Si}}$. Note also that the minima of the valley splitting oscillations in Fig. 4(d) do not reach zero, as it is instead the case for Ge or Si quantum wells between SiGe barriers.[34] The rationale for this is that the two Si interfaces in the tube are not identical, being formed by H atoms on one side and Ge atoms on the other side.

Another relevant aspect of the VS is the damping of the oscillations observed in the region of large $N_{\mathrm{Si}}$ of Fig. 4(d). This effect is due to the fact that upon increasing the tube thickness, the confinement energy is reduced and therefore the wave function becomes completely confined by the triangular potential profile. The consequence is that the electron wave functions vanish before reaching the (sharp) left Si-H interface. Then, the VS does not depend anymore on the exact value of $N_{\mathrm{Si}}$ but only on the slope of the band profile, i.e., the strength of the effective electric field. For large values of $N_{\mathrm{S}i}$, VS oscillations are completely damped (see Fig. 4), with amplitude decreasing as $N_{\mathrm{Si}}^{-1}$. To justify this fact, we remind that for triangular confining potentials, the VS amplitude is proportional to the slope of the triangular potential.[30,50] In our case, this slope is eventually determined by the requirement $R_1 = R_{\min}$; we have numerically verified that this condition determines a slope of the strain profile, $d\epsilon_{\rho\rho}(\rho)/d\rho$, which is indeed proportional to $N_{\mathrm{Si}}^{-1}$.

From Fig. 4(d) we deduce that damping of the VS oscillations can also be obtained for fixed value $N_{\mathrm{Si}}$ but decreasing $R_1$ [vertical orange line in Fig. 4(d)]. To gain further insight in the role of curvature on VS we show in Fig. 4(e) the VS as a function of the internal radius $R_1$, for three fixed values of $N_{\mathrm{Si}}$. As before, the internal radius is evaluated for different values of $N_{\mathrm{Ge}}$ by minimization of the elastic energy. The main trend in Fig. 4(e) is an increase of the VS for small tube radii, while for $R_1 \to \infty$ the VS tends to the asymptotic value obtained for the planar slab. Indeed, for small $R_1$ values the confining potential is again triangular and the slope of the band-edge potential increases as $R_1$ diminishes [see also Figs. 4(a)–4(c)]. The corresponding effect in biased triangular Si/SiGe QW systems is the (almost) linear dependence of the VS on the strength of the applied field. Note again that for small $R_1$ the wave functions tend to become insensitive to the actual well width, as apparent from the superposition of the red and green curves in the left portion of Fig. 4(e). On the contrary, for large radii, the strain is reduced, so that the band profile tends to a square potential well and both the H-Si and the Si-Ge interfaces are felt by the electron wave functions. Consequently, as already discussed, we expect a significant dependence of the VS on the parity of $N_{\mathrm{Si}}$, and in fact for large $R_1$ the VSs of the tubes with $N_{\mathrm{Si}} = 58$ and 59 tend to different values.

## IV. CONCLUSIONS

In conclusion, we have theoretically and numerically investigated the electronic band structure of Si/Ge rolled-up nanotubes. Equilibrium tube geometry has been obtained minimizing the total elastic energy of the tubes by means of the continuum elasticity theory. The electronic states have been calculated by a nearest-neighbor $sp^3d^5s^*$ tight-binding model, suitably adapted to the cylindrical geometry. The adopted atomistic approach allows us to carefully consider strain conditions and interface effects and provides a description of the electronic states over all the Brillouin zone of the tube. In particular, we have presented here the multivalley structure of the conduction band and the intervalley splitting of the tube levels at its bottom. Our results show that the $\Delta$ band-edge states are inequivalent. This degeneracy removal has been interpreted in terms of the confinement effects and of the action on the electronic spectrum of the nonbiaxial strain fields induced by the tube curvature. We have also discussed the importance of the curvature in affecting the valley splitting magnitude, demonstrating that the role of the curvature-induced strain on the VS is analogous to that of a vertical electric field applied to an equivalent quantum well planar structure. This effect is to be attributed to the presence of a strain gradient for $\epsilon_{\rho\rho}(\rho)$ along the $\rho$ direction associated to the curvature which, in the Si and Ge regions, is approximately constant. The results of this work will be useful for a deeper understanding of the physical mechanisms that determine the electronic states in rolled-up tubes, toward the design of novel devices with tailored functionality.

## ACKNOWLEDGMENTS

One of the authors (G.P.) gratefully acknowledges financial support from Scuola Normale Superiore, and the kind hospitality at the Institute for Integrative Nanosciences (IFW Dresden). The work was financially supported by the DFG FOR 1154 "Towards Molecular Spintronics," the DFG priority program "Nano-Thermoelektrik," and the US Air Force Office of Scientific Research MURI program under Grant No. FA9550-09-1-0550.

## APPENDIX: STRAIN EFFECTS IN THE CONDUCTION BAND FOR THE CASE OF THE $\mathrm{Si}_{16}/\mathrm{Ge}_9$ TUBE

In order to better understand the role of strain on the electronic states of SiGe rolled-up nanotubes, and the spatial localization of the different kinds of $\Delta$ states, we discuss in this Appendix an exemplificative case, analyzing the tube with $N_{\mathrm{Si}} = 16$ and $N_{\mathrm{Ge}} = 9$ and internal radius $R_1 = 49.1$ nm, whose band structure is shown in Fig. 3. In particular, we show in Fig. 5 the diagonal components of the strain tensor as a function of the radial coordinate $\rho$, and the near-gap conduction wave functions for the three $\Delta$ valleys, with the corresponding band-edge profiles. The band edges are defined

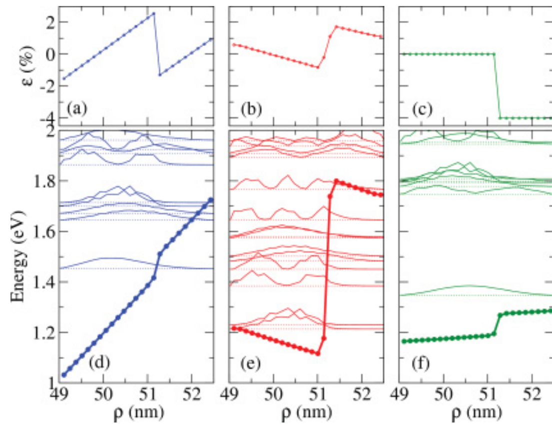


FIG. 5. (Color online) (a)–(c) Diagonal strain components $\epsilon_{\theta\theta}(\rho)$, $\epsilon_{\rho\rho}(\rho)$, $\epsilon_{zz}(\rho)$, respectively, as a function of the radial coordinate $\rho$, for a $Si_{16}/Ge_9$ tube with internal radius $R_1 = 49.1$ nm. (d)–(f) Band-edge profiles (thick lines) for the $\Delta_\theta$, $\Delta_\rho$, $\Delta_z$ valleys, respectively, and square moduli of their wave functions, calculated at the $k$ points corresponding to the valley minima (see Fig. 3).

as the energies of the respective states in a bulk system with a diagonal strain tensor with (in general) different strains along $x$, $y$, and $z$. These strains are taken equal to the local strain components in the tube. Note that the band-edge profiles that we show are just a guide for the interpretation of the results, but are not directly used in the calculation of the electronic states of the system, which instead result from the diagonalization of the TB Hamiltonian.

In the $\theta$ direction, the lattice constant is related to the radius $\rho$ by $a_\theta = C\rho$, where $C$ is a suitable positive constant obtained from the structural relaxation. Then, the strain increases linearly with $\rho$, and has a sudden (downward) jump at the Si/Ge interface since $\epsilon_{\theta\theta} = \frac{a_\theta - a_i}{a_i}$ where $i$ is Si or Ge depending on which layer we are considering [see Fig. 5(a)]. The behavior of the $\epsilon_{\rho\rho}$ component is expected to be opposite the one of the $\epsilon_{\theta\theta}$ component due to the Poisson's effect. Indeed, $\epsilon_{\rho\rho}(\rho)$ has a decreasing behavior with an upward discontinuity at the inner interface [see Fig. 5(b)]. Finally as already discussed we assume $a_z = a_{\rm Si}$: therefore the $\epsilon_{zz}$ component is identically zero in the Si portion of the tube, while it assumes the value $\frac{a_{\rm Si} - a_{\rm Ge}}{a_{\rm Ge}} \approx -4\%$ in the Ge region [see Fig. 5(c)].

In Figs. 5(d)–5(f) we show the band-edge profiles for the $\Delta_\theta$, $\Delta_\rho$, $\Delta_z$ valleys, respectively, and the square modulus of the corresponding wave functions, calculated at the $k$ points corresponding to the valley minima (see Fig. 3).

Since a compressive (tensile) diagonal component of the strain along a given direction determines a lowering (rise) in energy of the band edge along the $\Delta$ line in the same direction, each band-edge profile as a function of $\rho$ follows closely the behavior of the corresponding strain component, as long as we are within the same layer. At the interface, the jump of the strain produces a discontinuity in the band profile that has to be added to the conduction-band offset between the $\Delta$ bands of Si and Ge. Since this offset is positive for Ge with respect to Si, the net result is that the discontinuity almost cancels out for the $\Delta_\theta$ and $\Delta_z$ profiles, since both $\epsilon_{\theta\theta}$ and $\epsilon_{zz}$ have a downward discontinuity. On the contrary, the discontinuity of the $\Delta_\rho$ profile is enhanced since the $\epsilon_{\rho\rho}$ discontinuity is positive when going from Si to Ge.

The three band-edge profiles reported in Fig. 5 determine the behavior of the respective wave functions. Due to the large slope of the $\Delta_\theta$ profile, its lowest-energy wave function is mainly confined in the Si region, while the $\Delta_z$ state is instead almost evenly distributed over the whole tube [compare Figs. 5(d) and 5(f)]. The narrower region in which the $\Delta_\theta$ wave function is localized results in a larger confinement energy even if both states have the same confinement mass; as a consequence, the bottom $\Delta_\theta$ state is at a higher energy than the bottom $\Delta_z$ state. For what concerns the $\Delta_\rho$ valley the low-energy states, and in particular the ground-state valley splitting (VS) doublet, are strongly confined in the Si layer due to the large discontinuity of the $\Delta_\rho$ profile at the Si/Ge interface. For this reason, in Sec. III we discuss the VS as a function of $N_{\rm Si}$, since the number of Ge layers influences the VS only through its control of the tube radius and as a consequence of the slope of the band-edge profile in the Si region. Finally, for an experimental nondestructive determination of the local structure and strain state of the tubes, we refer to Ref. 51.

---

*Present address: Theory and Simulation of Materials (THEOS), École Polytechnique Fédérale de Lausanne, Station 12, 1015 Lausanne, Switzerland; giovanni.pizzi@epfl.ch

†Present address: Department of Electrical and Computer Engineering, Naresuan University, Phitsanulok 65000, Thailand.

[1] O. Gülseren, T. Yildirim, and S. Ciraci, Phys. Rev. B **65**, 153405 (2002).

[2] S. B. Fagan, L. B. da Silva, and R. Mota, Nano Lett. **3**, 289 (2003).

[3] V. M. Osadchii and V. Y. Prinz, Phys. Rev. B **72**, 033313 (2005).

[4] Y. F. Mei, S. Kiravittaya, M. Benyoucef, D. J. Thurmer, T. Zander, C. Deneke, F. Cavallo, A. Rastelli, and O. G. Schmidt, Nano Lett. **7**, 1676 (2007).

[5] S. Ono and H. Shima, Phys. Rev. B **79**, 235407 (2009).

[6] Y. F. Mei, S. Kiravittaya, S. Harazim, and O. G. Schmidt, *3rd IEEE International NanoElectronics Conference (INEC)*, Mat. Sci. Eng. R: Reports **70**, 209 (2010).

[7] C. Ortix, S. Kiravittaya, O. G. Schmidt, and J. van den Brink, Phys. Rev. B **84**, 045438 (2011).

[8] P. Cendula, S. Kiravittaya, I. Mönch, J. Schumann, and O. G. Schmidt, Nano Lett. **11**, 236 (2011).

[9] O. G. Schmidt and K. Eberl, Nature (London) **410**, 168 (2001).

[10] S. V. Golod, V. Y. Prinz, V. I. Mashanov, and A. K. Gutakovsky, Semicond. Sci. Technol. **16**, 181 (2001).

[11] J. Zang, M. Huang, and F. Liu, Phys. Rev. Lett. **98**, 146102 (2007).

[12] X. Li, J. Phys. D **41**, 193001 (2008).

[13] M. Huang, F. Cavallo, F. Liu, and M. G. Lagally, Nanoscale **3**, 96 (2011).

[14] F. Cavallo, R. Songmuang, and O. G. Schmidt, Appl. Phys. Lett. **93**, 143113 (2008).

[15] F. Chen, C. Euaruksakul, Z. Liu, F. J. Himpsel, F. Liu, and M. G. Lagally, J. Phys. D **44**, 325107 (2011).

[16]C. C. Bof Bufon, J. D. Cojal González, D. J. Thurmer, D. Grimm, M. Bauer, and O. G. Schmidt, Nano Lett. **10**, 2506 (2010).
[17]K. Dietrich, C. Strelow, C. Schliehe, C. Heyn, A. Stemmann, S. Schwaiger, S. Mendach, A. Mews, H. Weller, D. Heitmann, and T. Kipp, Nano Lett. **10**, 627 (2010).
[18]E. J. Smith, S. Schulze, S. Kiravittaya, Y. Mei, S. Sanchez, and O. G. Schmidt, Nano Lett. **11**, 4037 (2011).
[19]S. Sanchez, A. N. Ananth, V. M. Fomin, M. Viehrig, and O. G. Schmidt, J. Am. Chem. Soc. **133**, 14860 (2011).
[20]Z. Tian, V. Veerasubramanian, P. Bianucci, S. Mukherjee, Z. Mi, A. G. Kirk, and D. V. Plant, Opt. Express **19**, 12164 (2011).
[21]C. C. Bof Bufon, J. D. Arias Espinoza, D. J. Thurmer, M. Bauer, C. Deneke, U. Zschieschang, H. Klauk, and O. G. Schmidt, Nano Lett. **11**, 3727 (2011).
[22]G. Ferrari and G. Cuoghi, Phys. Rev. Lett. **100**, 230403 (2008).
[23]G. Ferrari, A. Bertoni, G. Goldoni, and E. Molinari, Phys. Rev. B **78**, 115326 (2008).
[24]C. Ortix and J. van den Brink, Phys. Rev. B **81**, 165419 (2010).
[25]N. V. Demarina and D. A. Grützmacher, Appl. Phys. Lett. **98**, 192109 (2011).
[26]K. Kubota, P. O. Vaccaro, N. Ohtani, Y. Hirose, M. Hosoda, and T. Aida, Physica E **13**, 313 (2002).
[27]S. Mendach, R. Songmuang, S. Kiravittaya, A. Rastelli, M. Benyoucef, and O. G. Schmidt, Appl. Phys. Lett. **88**, 111120 (2006).
[28]A. B. Fowler, F. F. Fang, W. E. Howard, and P. J. Stiles, Phys. Rev. Lett. **16**, 901 (1966).
[29]D. Z.-Y. Ting and Y.-C. Chang, Phys. Rev. B **38**, 3414 (1988).
[30]G. Grosso, G. Pastori Parravicini, and C. Piermarocchi, Phys. Rev. B **54**, 16393 (1996).
[31]T. B. Boykin, G. Klimeck, M. A. Eriksson, M. Friesen, S. N. Coppersmith, P. von Allmen, F. Oyafuso, and S. Lee, Appl. Phys. Lett. **84**, 115 (2004).
[32]M. A. Wilde, M. Rhode, C. Heyn, D. Heitmann, D. Grundler, U. Zeitler, F. Schäffler, and R. J. Haug, Phys. Rev. B **72**, 165429 (2005).
[33]A. Valavanis, Z. Ikonić, and R. W. Kelsall, Phys. Rev. B **75**, 205332 (2007).
[34]M. Virgilio and G. Grosso, Phys. Rev. B **75**, 235428 (2007).
[35]M. Virgilio and G. Grosso, Phys. Rev. B **79**, 165310 (2009).
[36]S. Srinivasan, G. Klimeck, and L. P. Rokhinson, Appl. Phys. Lett. **93**, 112102 (2008).
[37]B. E. Kane, Nature (London) **393**, 133 (1998).
[38]N. Kharche, M. Prada, T. B. Boykin, and G. Klimeck, Appl. Phys. Lett. **90**, 092109 (2007).
[39]For very small tubes, this method can give a slightly larger tube radius (lower curvature effect) as compared with atomistic calculations, even if the discrepancy is always tiny for all systems considered. More details of the comparison between these two methods will be published elsewhere.
[40]*Semiconductors: Group IV Elements and III-V Compounds*, edited by O. Madelung (Springer, New York, 1991).
[41]M. Grundmann, Appl. Phys. Lett. **83**, 2444 (2003).
[42]A. Malachias, C. Deneke, B. Krause, C. Mocuta, S. Kiravittaya, T. H. Metzger, and O. G. Schmidt, Phys. Rev. B **79**, 035301 (2009).
[43]G. Grosso and G. Pastori Parravicini, *Solid State Physics* (Academic, San Diego, 2000).
[44]M. O. Nestoklon, L. E. Golub, and E. L. Ivchenko, Phys. Rev. B **73**, 235334 (2006).
[45]T. B. Boykin, G. Klimeck, M. Friesen, S. N. Coppersmith, P. von Allmen, F. Oyafuso, and S. Lee, Phys. Rev. B **70**, 165325 (2004).
[46]T. B. Boykin, N. Kharche, and G. Klimeck, Phys. Rev. B **77**, 245320 (2008).
[47]Y. M. Niquet, D. Rideau, C. Tavernier, H. Jaouen, and X. Blase, Phys. Rev. B **79**, 245201 (2009).
[48]Y. Zheng, C. Rivas, R. Lake, K. Alam, T. Boykin, and G. Klimeck, IEEE Trans. Electron Devices **52**, 1097 (2005).
[49]Y. S. Yukecheva, G. Mussler, V. Shushunova, A. Weber, E. Deckardt, V. Y. Prinz, and D. Grützmacher, Semicond. Sci. Technol. **23**, 105007 (2008).
[50]M. Friesen, S. Chutia, C. Tahan, and S. N. Coppersmith, Phys. Rev. B **75**, 115318 (2007).
[51]B. Krause, C. Mocuta, T. H. Metzger, C. Deneke, and O. G. Schmidt, Phys. Rev. Lett. **96**, 165502 (2006).